UC Berkeley
UC Berkeley Previously Published Works

Title

Trapped bubbles keep pumice afloat and gas diffusion makes pumice sink

Permalink

https://escholarship.org/uc/item/5032h14q

Authors

Fauria, Kristen E
Manga, Michael
Wei, Zihan

Publication Date

2017-02-01

DOI

10.1016/j.epsl.2016.11.055

Peer reviewed

Trapped bubbles keep pumice afloat and gas diffusion makes pumice sink

Author links open overlay panel Kristen E.Fauria[a] Michael Manga[a] Zihan Wei[ab]
Show more

Highlights

- X-ray microtomography shows that hot (500 °C) and ambient-temperature pumice trap gas.

- The size distributions of trapped gas clusters match percolation theory.

- Gas trapping can explain why pumice floats on water.

- Pumice sinks because of outward diffusion of trapped gas.

Abstract

Pumice can float on water for months to years – long enough for pumice to travel across oceans and facilitate the spread of species. Long-lived pumice floatation is unexpected, however, because pumice pores are highly connected and water wets volcanic glass. As a result, observations of long floating times have not been reconciled with predictions of rapid sinking. We propose a mechanism to resolve this paradox – the trapping of gas bubbles by water within the pumice. Gas trapping refers to the isolation of gas by water within pore throats such that the gas becomes disconnected from the atmosphere and unable to escape. We use X-ray microtomography to image partially saturated pumice and demonstrate that non-condensable gas trapping occurs in both ambient temperature and hot (500 °C) pumice. Furthermore, we show that the size distribution of trapped gas clusters matches predictions of percolation theory. Finally, we propose that diffusion of trapped gas determines pumice floatation time. Experimental measurements of pumice floatation support a diffusion control on pumice buoyancy and we find that floatation time τ scales as $\tau \propto \frac{L^2 \theta^2}{D}$ where L is the characteristic length of pumice, D is the gas–water diffusion coefficient, and θ is pumice water saturation. A mechanistic understanding of pumice floatation is a step towards understanding how

pumice is partitioned into floating and sinking components and provides an estimate for the lifetime of pumice rafts in the ocean.

Keywords

buoyancy
capillary processes
percolation theory
submarine volcanism
X-ray microtomography

Notation

v	velocity		p	volume–area coefficient
μ	dynamic viscosity		τ	pumice floatation timescale
γ	surface tension		D_{eff}	effective diffusion coefficient
ρ	density		θ	water saturation
g	gravity		D	liquid–gas diffusion coefficient
κ	permeability		d	mean pore throat diameter
ϕ	connected porosity		P	pressure
h	height		R	pore throat radius
V_w	volume of water absorbed		T	temperature
t	time		L_w	glass wall thickness
S_a	pumice surface area		D_w	water thermal diffusivity
n	number of occurrences		T_i	initial temperature
s	sites or pores		T_f	final temperature
β	power law coefficient		V_i	initial volume
a	spatial dimension		V_f	final volume
f	fractal dimension a cluster		ξ	gas saturation
s_{max}	maximum size of a trapped gas cluster		ξ_i	initial gas saturation
L	pumice diameter		ξ_*	neutral buoyancy gas saturation
A	surface area of trapped gas clusters		ρ_r	glass density
V	trapped gas volume		ρ_l	liquid density

1. Introduction

Pumice is a highly vesicular volcanic rock with a porosity high enough that it can float. Rafts of volcanic pumice can transit lakes and oceans and circle the globe (e.g., Richards, 1958, Risso et al., 2002, Bryan et al., 2004, von Lichtan et al., 2016). For example, pumice from the 1952 eruption of Volcán Barcena on Isla San Benedicto, 600 km west of Mexico, floated for at least 560 days and drifted over 8700 km (Richards, 1958). The 2012 eruption of Havre submarine volcano created a 1.5 km^3 pumice raft that spread over 550,000 km^2 within three months (Carey et al., 2014, Jutzeler et al., 2014). Pumice rafts have been shown to facilitate the dispersal of species such as barnacles, corals, algae, and gastropods (Bryan et al., 2012) because marine organisms grow on, and ocean currents advect, pumice (Richards, 1958, Jokiel, 1984, Bryan et al., 2004). While pumice rafts are relatively common and it is well known that ambient temperature pumice can float for long periods of time, the enduring buoyancy of pumice is surprising because pumice pores are almost entirely connected and water wets pumice (Whitham and Sparks, 1986, Vella and Huppert, 2007). Quantitative models for pumice saturation predict that ambient temperature pumice should sink orders of magnitude more rapidly than is observed (Vella and Huppert, 2007). The floatation time discrepancy between observations and the Vella and Huppert (2007) model suggests that simple gas displacement by an infiltrating water front is not sufficient to explain why ambient temperature pumice can float for years.

By comparison to ambient temperature pumice, hot pumice (e.g., >300 °C) sinks almost immediately and the tendency for air-filled pumice to sink increases with pumice temperature (Whitham and Sparks, 1986, Dufek et al., 2007, Allen et al., 2008, Jutzeler et al., 2016). Rapid water ingestion by hot pumice has been attributed to cooling-induced gas contraction (Whitham and Sparks, 1986, Cashman and Fiske, 1991, Allen et al., 2008) and hydrodynamic instabilities due to steam generation (Dufek et al., 2007). Air-filled hot pumice placed in water does not, however, completely saturate even at high (500 °C) temperatures (Allen et al., 2008). As a result, we wish to understand how gas remains within initially hot pumice and what differences and similarities exist between saturation of ambient temperature and hot non-condensable gas filled pumice. Pumice, with porosities of 50 to >90 percent, is a porous medium. Water saturation of pumice is an example of two-phase flow in porous media and requires the replacement of a defending fluid (air or magmatic gases) with an invading fluid (liquid water). Two-phase flow in porous media has been widely studied in the context of the vadose zone, oil recovery, CO$_2$ sequestration, and gas sparging. In addition, water infiltration of pumice is a manifestation of a particular type of two-phase flow, imbibition, because water is the wetting phase. During imbibition the arrangement of fluid, or wetting pattern,

can range from one where nearly all the pores are filled with the invading fluid to one where the defending fluid remains trapped in clusters (e.g., Lenormand and Zarcone, 1984). Trapped gas clusters (Fig. 1), pockets of non-wetting fluid that are surrounded by the wetting fluid, are not only characteristic of two-phase flow in porous media but are very difficult to mobilize because of surface tension. Indeed, gas trapping is a mechanism employed for long term CO_2 sequestration (e.g., Ide et al., 2007, Benson and Cole, 2008).
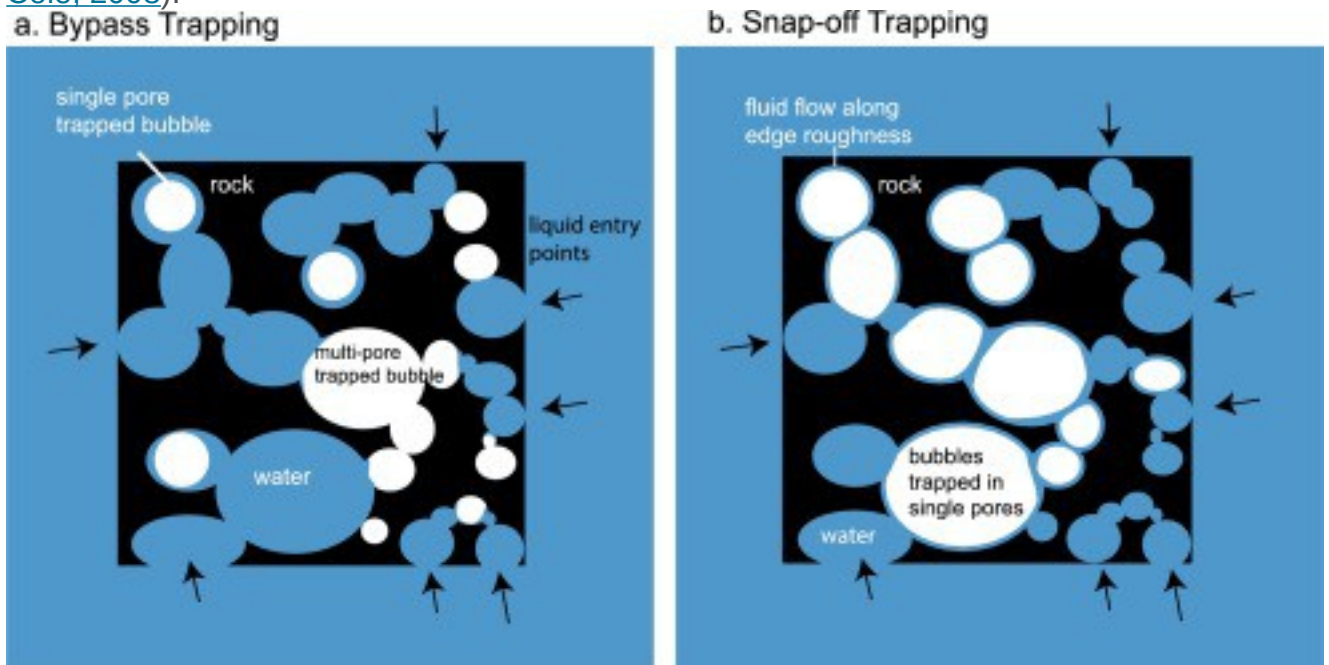
1. Download high-res image (228KB)
2. Download full-size image

Fig. 1. Mechanisms of gas trapping. Illustrations of gas trapping by (a) bypass and (b) snap-off trapping in pumice with connected pores. In both cases capillary forces draw water into pores such that water completely surrounds the gas phase and the gas is unable to escape.

We hypothesize that pumice floats for long periods of time because of the occurrence of gas trapping (either air or non-condensable magmatic gases) in isolated gas clusters during water infiltration. We use X-ray microtomography to test the hypotheses that gas trapping occurs in both hot and ambient temperature pumice, that gas trapping can result in a high enough residual gas saturations to keep pumice afloat, and that percolation theory can describe gas trapping in pumice. While trapped gas may buoy pumice, we hypothesize that the outward diffusion of gas trapped in bubbles eventually causes pumice to sink. We test this gas diffusion hypothesis by conducting experiments where we measure the floatation time of dry and ambient temperature

pumice on artificial seawater in a controlled laboratory setting. We then compare our results and pumice floatation times from four other studies with a prediction for pumice floatation time based on gas-diffusion out of a porous medium.

1.1. Gas trapping in porous media

Gas trapping has been observed in experiments, dictates wetting patterns, and controls residual non-wetting saturation of porous media (e.g., Blunt and Scher, 1995, Iglauer et al., 2013, Geistlinger and Mohammadian, 2015). A key element that promotes gas trapping is the slow advance of the invading fluid such that capillary forces dominate over viscous forces. In other words, the Capillary number

$$(1) \quad Ca = \frac{v\mu}{\gamma},$$

where v is the characteristic velocity, μ is the wetting fluid viscosity, and γ is surface tension on the interface between the two fluids, is very small, $Ca \ll 1$ (Lenormand and Zarcone, 1984, Wilkinson, 1984, Blunt and Scher, 1995).

We calculate a Capillary number for water infiltration into dry pumice using $\mu = 10^{-3} Pa\,s$ for the viscosity of water at room temperature, $\gamma = 0.072 N\,m^{-1}$ for the surface tension at the air–water interface, and by estimating the velocity of water infiltrating pumice using Darcy's law. For pumice floating on water, the maximum head gradient is set by the hydrostatic pressure at the bottom edge of the pumice and the capillary pressure. By assuming a constant pore radius and a hemispherical gas–water meniscus we can write the liquid velocity as

$$(2) \quad v = \frac{\kappa}{\mu \phi}\left(\rho g h + \frac{2\gamma}{R}\right),$$

where κ is permeability, ϕ is connected porosity, ρ is water density, g is gravity, h is the height of pumice in water, and R is pore throat radius. Pumice porosities can vary widely, but typical values are 50 to 90 percent (pumice with rock equivalent densities between 2.4 and 3.0 g cm^{-3} must have porosities of at least 58 to 67 percent, respectively, to initially float). Pumice permeabilities are more difficult to estimate, but measured values range from 10^{-14}–$10^{-10} m^2$ (e.g., Klug and Cashman, 1996, Tait et al., 1998, Saar and Manga, 1999, Klug et al., 2002; Rust and Cashman, 2004, Rust and Cashman, 2011; Mueller et al., 2005; Wright et al., 2006, Wright et al., 2009; Degruyter et al., 2010). We note that permeability may also be a function of saturation, i.e., relative permeability is not unity. We consider pumice that is immersed 0.01–1 m in water and pores that have radii of 0.1–0.001 mm. From these input parameters, $3.8 \times 10^{-11} < Ca < 4.3 \times 10^{-4}$, which shows that capillary forces dominate in pumice.

We also use pumice saturation measurements from [Whitham and Sparks (1986)](#) to estimate water infiltration velocities according to,

$$(3) \quad v = \frac{\Delta V_w}{\Delta t \, S_a \phi}$$

where V_w is the volume of absorbed water, t is time, S_a is pumice surface area, and ϕ is connected porosity. We estimate S_a by assuming the pumice [clasts](#) are spherical. Fourteen pumice saturation measurements by [Whitham and Sparks (1986)](#) reveal average initial infiltration velocities over the first five minutes of water exposure of $2.74 \pm 0.97 \times 10^{-2} \, cm \, hr^{-1}$ and Capillary numbers of $7.62 \pm 2.69 \times 10^{-8}$. These Ca estimates indicate that capillary forces dominate. Thus, the saturation of pumice should be considered at the [pore scale](#) and may lead to gas trapping. In the next sections we introduce two mechanisms that allow gas trapping to occur, the percolation models that simulate them, and the gas-trapping predictions percolation theory makes.

1.1.1. Bypass trapping

Bypass trapping ([Fig. 1](#)a) causes trapping through the sequential filling of pore throats such that the defending fluid becomes surrounded by the invading fluid before it can escape (e.g., [Chatzis et al., 1983](#)). Invasion percolation models simulate bypass trapping by (1) representing the porous medium as a network of spheres (pores) and cylinders (pore throats); (2) prescribing a capillary entry pressure for each throat and pore; and (3) filling throats and pores from highest to lowest pressure. As a result, a pore or series of pores with low capillary pressures may be completely surrounded before being filled and thus become trapped (but may contract or expand if compressible).

1.1.2. Snap-off trapping

Snap-off trapping occurs because for very [low flow](#) rates (or capillary numbers) the wetting fluid can flow along edges of the pore walls due to [surface roughness](#) (e.g., [Lenormand and Zarcone, 1984](#)). This wall-hugging thin film can swell as the wetting fluid invades. As the film swells in the smallest throats, it completely displaces the non-wetting phase and can disconnect the non-wetting phase from any neighbors ([Fig. 1](#)b). Snap-off trapping is simulated by Bond percolation. When snap-off and bypass trapping are both possible, bypass trapping is favored because it occurs for higher capillary pressures.

1.1.3. Percolation model predictions

Both invasion and bond percolation theory make predictions about the size distribution of residual trapped gas clusters. Because percolation systems are scale invariant at

the critical point (when fully percolated), the number of occurrences, n(s), of trapped gas clusters containing s sites or pores scales according to a power-law,

(4) $n(s) \sim s^{-\beta}$,

where $\beta = a + ff$ and a is the spatial dimension and f is the fractal dimension of the cluster. In 3D: a=3, f=2.52, and β=2.19 (Stauffer, 1979, Wilkinson and Willemsen, 1983). The maximum size of the trapped gas cluster is limited by the samples size, L, $s_{max} \sim L^f$ (Wilkinson, 1986). Experimental studies of imbibition in porous media have shown that trapped gas size distributions match Equation (4) (e.g., Geistlinger and Mohammadian, 2015). Examining the size distribution of trapped gas bubbles in a natural system, such as pumice, can therefore help distinguish if percolation theory (either Bond or Invasion) applies.

2. X-ray microtomography

X-ray microtomography (μXRT) allows us to see both the internal structure of pumice (e.g., Polacci et al., 2006, Wright et al., 2006, Degruyter et al., 2010, Giachetti et al., 2011, Voltolini et al., 2011, Carey et al., 2013) and, when multiple fluids are present within the pores, the distribution of those fluids (e.g., Wildenschild et al., 2002). We use μXRT to (1) test the hypothesis that gas trapping occurs in pumice; (2) determine if percolation theory can describe the size distribution of trapped gas; (3) examine the size distribution of trapped gas for insights into the mechanisms (bypass or snap-off trapping) that occur in pumice.

2.1. Experimental set-up

We used μXRT to image the internal distribution of liquid and air in six uncut pumice clasts. Before the μXRT, we conducted saturation experiments on ambient temperature and hot (500 °C) pumice from Santa Maria, Guatemala and Medicine Lake, California (Table 1). We set ambient temperature pumice on a 13 wt% solution of potassium iodide (KI) for ~20 h such that the pumice could adsorb the liquid. KI, a common chemical dopant, increases contrast of the μXRT images (greatly improves the segmentation of air and water in the images), while maintaining a surface tension within 1% of water (Aveyard and Saleem, 1976; Wildenschild et al., 2002).

Table 1. μXRT samples (uncut clasts) and measurements.

Sample name	SM01	SM02	SM04	SM05	ML01	ML02
Sample description	1902 Santa Maria	1902 Santa Maria	1902 Santa Maria	1902 Santa Maria	Medicine Lake	Medicine Lake
Pumice mass (g)	0.07	0.19	0.13	0.04	0.15	0.76

Sample name	SM01	SM02	SM04	SM05	ML01	ML02
Pumice dimensions mm^3	9 × 4.5 × 4	11 × 7 × 4.5	11 × 6 × 5	6.5 × 3 × 3	9.5 × 5 × 5	5 × 5 × 4
Temperature	ambient	ambient	500 °C	500 °C	ambient	ambient
Ending buoyancy	floating	neutrally buoyant	not floating	not floating	not floating	barely floating
Porosity	0.70	NA	0.73	NA	0.63	0.67
Connected porosity	0.70	NA	0.73	NA	0.55	0.65
Liquid volume/total volume	0.30	NA	0.56	NA	0.13	0.31
Gas volume/total volume	0.40	0.36	0.17	0.13	0.50	0.36
Liquid saturation (liquid volume/pore volume)	0.43	NA	0.77	NA	0.21	0.46
Calculated wet density/KI density	0.86	NA	1.07	NA	0.83	0.93
Trapped gas bubble number density (cm^{-3})	9.6×10^5	3.0×10^6	4.4×10^6	4.2×10^6	7.2×10^6	2.3×10^6
Vesicle number density (cm^{-3})	8.3×10^6	NA	1.5×10^7	NA	9.6×10^6	5.3×10^6
β: Power law exponent	2.02	1.90	1.95	2.10	1.83	1.51
Smallest bubble fit to power law (mm^3)	5.9×10^{-5}	1.3×10^{-5}	2.3×10^{-5}	3.1×10^{-6}	1.3×10^{-4}	1.0×10^{-6}
p: Trapped bubble volume to surface area exponent	0.82	0.82	0.77	0.76	0.75	0.83
Size of analyzed volume (mm^3)	0.94	0.37	0.37	0.94	0.94	0.37

While µXRT analysis is done on subvolumes of larger clasts, we expect the subvolumes to be representative of the larger pumice in part because the pumice are relatively small (i.e., <1 g). Furthermore, the selected pumice samples do not have bread crust textures such that we expect differences between rim an internal porosities to be minimal.

We heated two of the pumice samples (SM04 and SM05) to 500 °C, quenched these pumice clasts in the KI dopant, and allowed them to stay in the solution for ∼10 min. All pumice pores were filled with air at the time of KI exposure. To preserve the internal fluid distributions for µXRT imaging, we then rapidly removed and encased the pumice in wax.

We carried out the µXRT imaging at the Lawrence Berkeley National Lab Advanced Light Source on beamline 8.3.2. We conducted the scans using 30 kev monochromatic X-rays and a 5X lens (resolution of 1.22µm/pixel). We used the TomoPy gridrec algorithm to reconstruct the 3D image stacks (Gürsoy et al., 2014).

To minimize ring artifacts, we selected a subvolume from each data set of either 0.37 or 0.94 mm³ for data processing. We used Fiji's Trainable Weka Segmentation plugin – which employs multiple machine learning algorithms – to segment air, water, and rock within each image sequence (Hall et al., 2009). To train classifiers for each image sequence, we manually outlined vesicles and trapped air on fifty different images. After checking and retraining the classifiers as necessary, we applied the trained classifiers across the images sequences to segment air and rock (thereby creating two sets of binarized image sequences for each sample).

We also made the image sequences binary by applying a greyscale threshold in Fiji, but determined that the machine learning method reduced the effect of annular ring artifacts and better preserved thin glass walls compared to the traditional threshold based binarization method. Despite the advantages of the machine learning method, two image sets (SM02 and SM05) had glass walls that were too thin to resolve and we do not report porosities or vesicle size distributions for these samples.

After we segmented each data set, we loaded the binary images into Avizo where we identified and quantified the volume, surface area, and orientation of individual bubbles and vesicles. Here we refer to the pores of the pumice (that can be filled with either gas or liquid) as vesicles and areas where the gas phase is present as bubbles. Because most samples had highly interconnected porosities, we separated connected vesicles using a watershed algorithm before measuring vesicles sizes and orientations (Supplementary information). No separation was applied to the gas bubbles. As a result, any observed and reported gas bubbles were truly isolated. We note, however, that some gas bubbles may appear connected (by one or two voxels) when they are not if glass walls are thinner than one pixel. To correct for very thin glass walls we use a "neighborhood" value of six in the Avizo labeling module such that bubbles must share at least one voxel face to be considered connected.

Errors in generating the bubble and vesicle size distributions stem from two main sources: (1) ring artifacts in the original greyscale image and (2) vesicle walls that are thinner than the voxel resolution and that may also lead to overestimates of connected porosity (Fig. S1). Through examination of twenty 2D images from each dataset, we estimate that ring artifacts result in the mischaracterization of gas or water in <1 volume percent of each pumice. While the machine learning method for image segmentation reduced the effects of ring artifacts compared to threshold based segmentation, it introduced a number of very small (artifact) bubbles and vesicles that do not contribute to the total volume fraction of pores or trapped gas. As a result, we filtered the data to

exclude any bubbles or vesicles with less than a 4.16 pixel radius or smaller than $10^{-6}mm^3$.
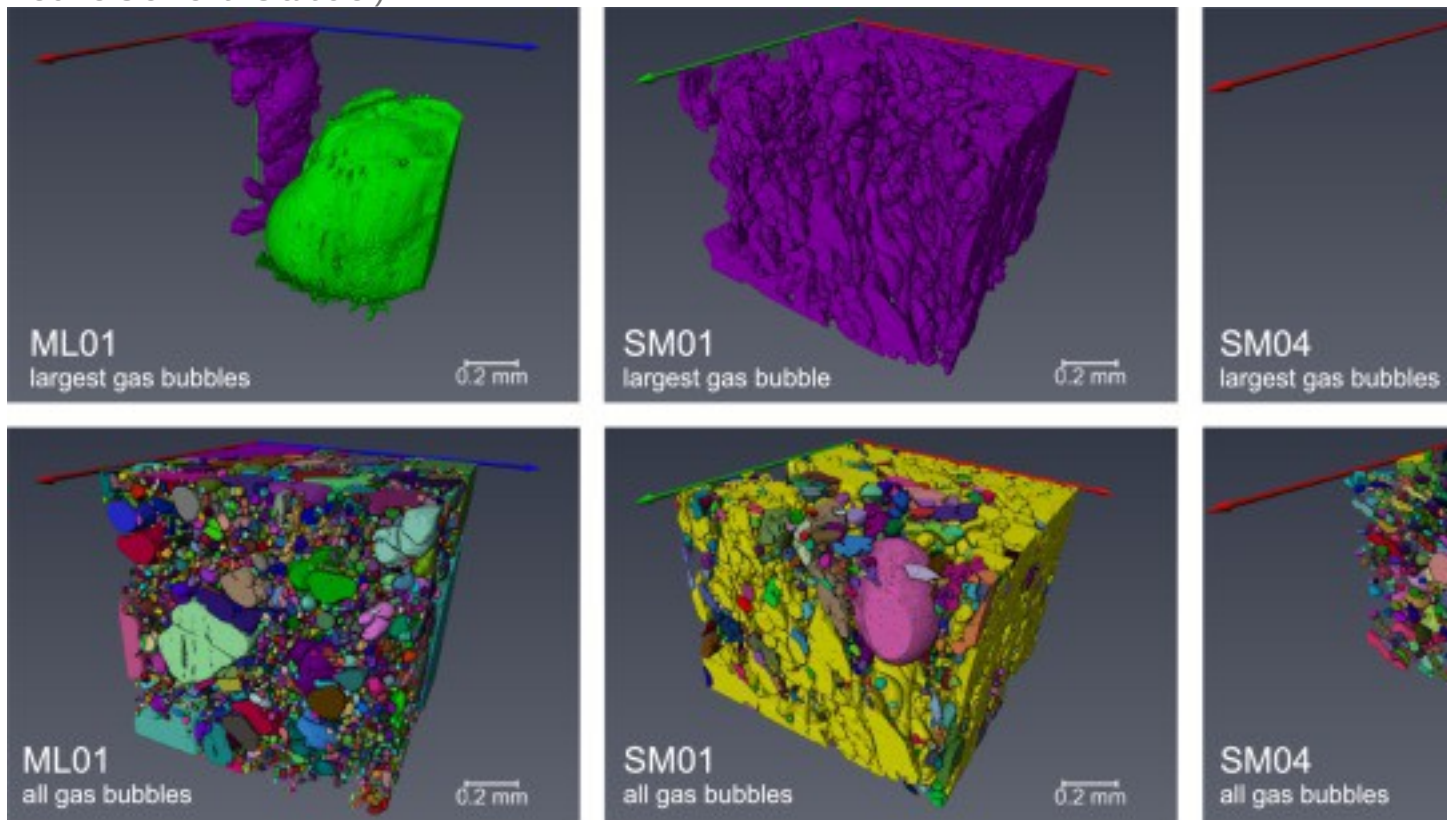
2.2. X-ray microtomography results

We find trapped gas clusters in all pumice we imaged (Fig. 2, Fig. 3). Trapped gas cluster size varies and gas clusters fill part of, single, and multiple vesicles (Fig. 2, Fig. 3). Because connected porosities for most samples are close to or equal to the total porosity, isolated gas pockets are due to trapping by liquid instead of isolation by rock (Table 1). Furthermore, we found that ambient temperature pumice contain larger volume percentages of trapped gas (36–50%) than the hot pumice (13 and 17%) (Table 1).

rock   gas   liquid
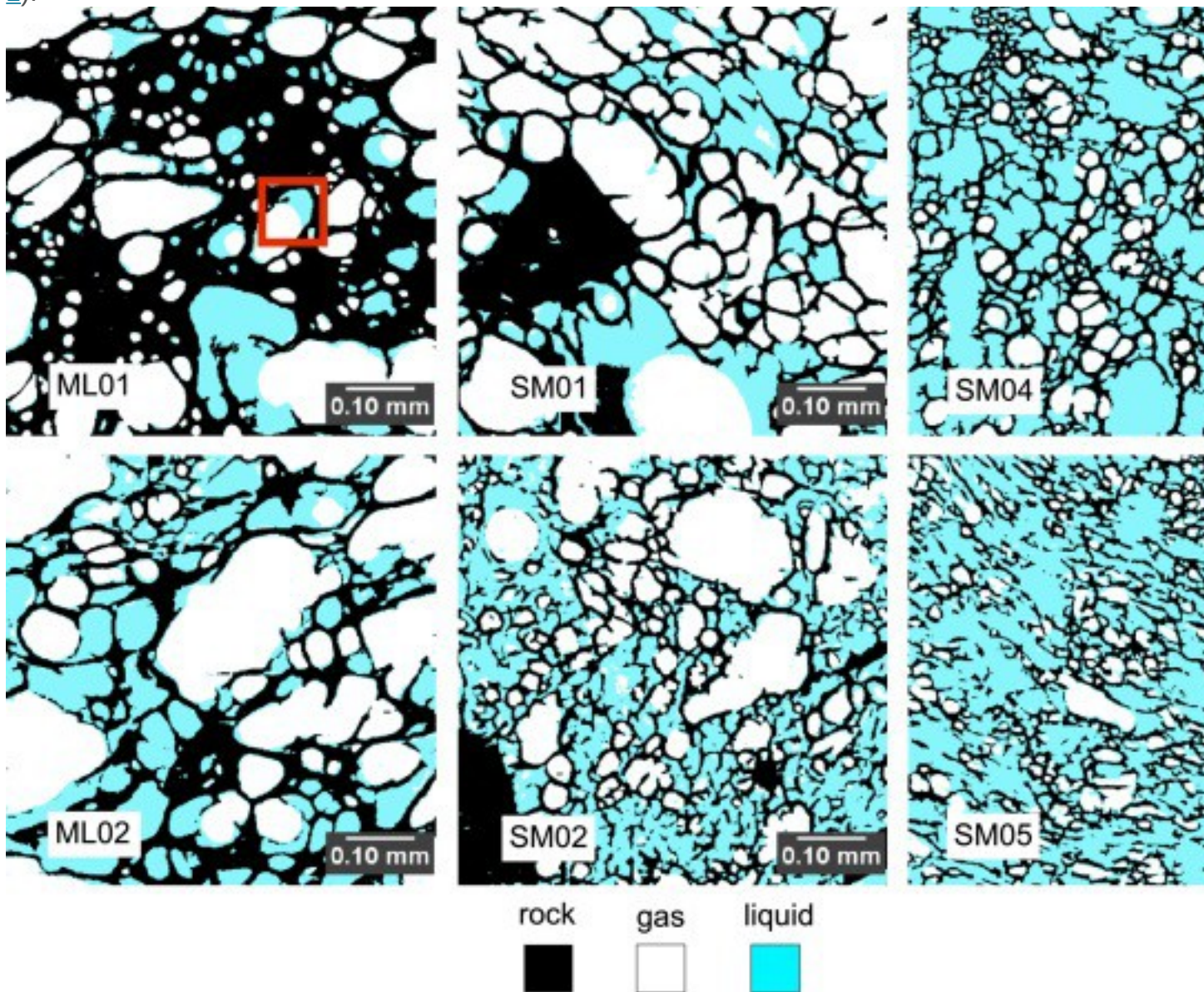
Fig. 2. X-ray microtomography images. 2D slices through μXRT images of pumice containing water and trapped gas. While hot pumice (SM04 and SM05) contain trapped gas, they hold smaller volume percentages compared to ambient temperature pumice. Contacts between rock, liquid, and gas demonstrate that the liquid is the wetting fluid (see red box). While glass walls are too thin to resolve in places (particularly in SM02 and SM05), we do not see any evidence in the μXRT that the thin glass walls in pumice are broken or damaged due to cleaning in an ultrasonic bath. (For interpretation of the references to color in this figure legend, the reader is referred to the web version of this article.)

Fig. 3. Shapes of trapped gas bubbles. 3D μXRT images of trapped gas bubbles within pumice. Colors in this figure are chosen at random to identify separate gas bubbles. The top rows show the largest gas bubbles and the bottom row shows all gas bubbles within a single pumice. A single interconnected gas bubbles extends throughout many pores in pumice SM01. (For interpretation of the references to color in this figure legend, the reader is referred to the web version of this article.)

We use μXRT measurements of phase (liquid and water) saturations to estimate pumice buoyancy, assuming glass densities of 2.4 g cm⁻³, and find that the observed trapped gas saturations are high enough to allow pumice to float. These density calculations match our observation that many of the pumice clasts were floating or neutrally buoyant when we encased them in wax. Our density calculation of ML01, however, does not match our observation that ML01 was not floating (Table 1). Discrepancies between observations and density estimages suggest that gas and liquid saturation within pumice is likely heterogeneous. Indeed, we visually observed areas of more and less gas saturation within μXRT images.

The size distributions of both trapped gas (black) and segmented pores (grey) are shown in Fig. 4. For the majority of samples (ML02, SM01, SM02, and SM05) at least a third of the trapped gas is contained within one large cluster. These clusters, in cases where the vesicle size distributions are known (SM01 and ML02), greatly exceed the maximum vesicle size and Fig. 3 shows how these largest trapped bubbles can extend throughout multiple vesicles. The trapped bubble size distributions, however, show that there are multiple modes of trapped bubbles sizes. In sample ML01, the trapped bubble size distribution mirrors the vesicle size distribution.
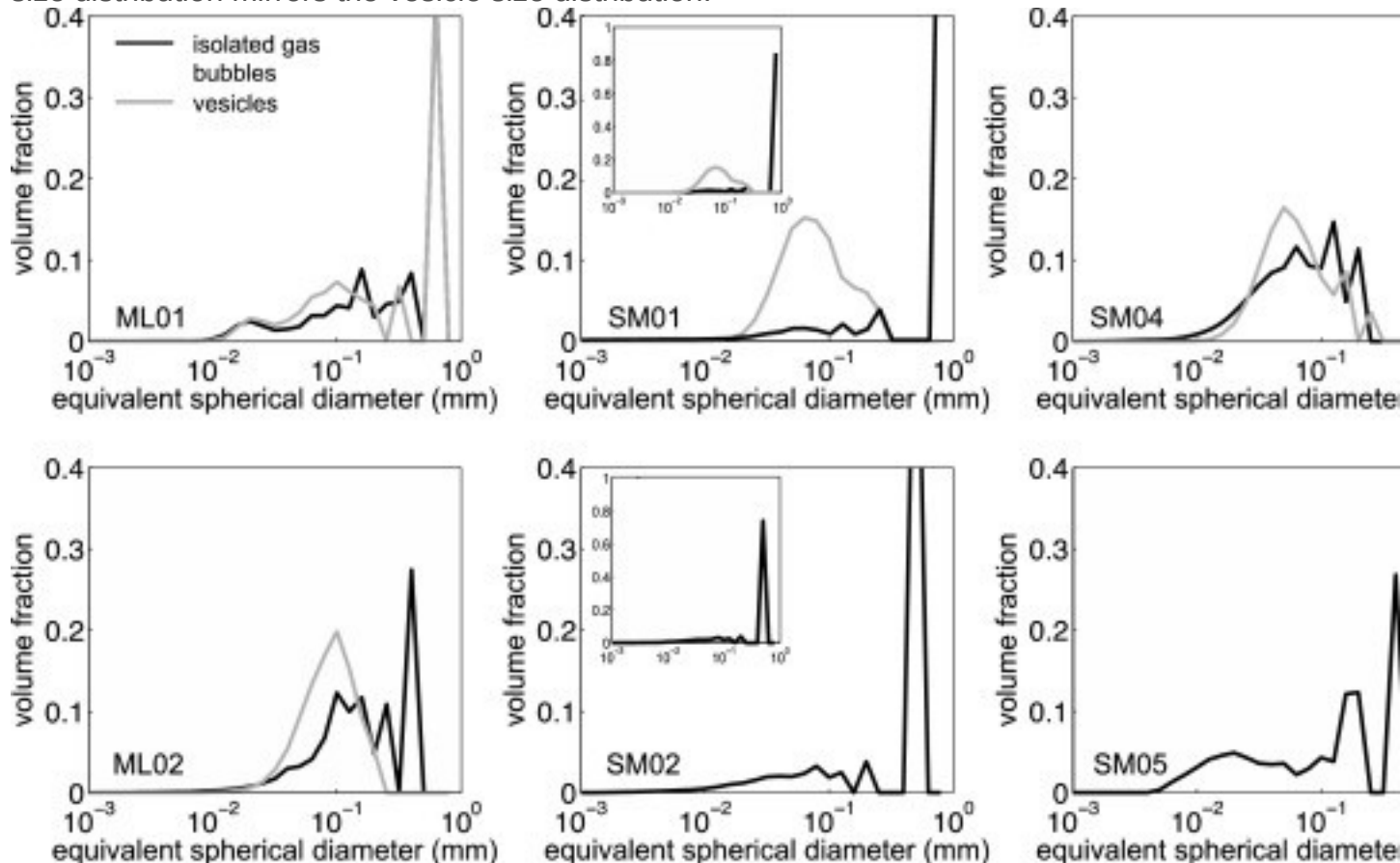
Fig. 4. Bubble and vesicle size distributions. Trapped gas bubbles, locations where only the gas is present, are shown in black, and vesicles, pumice pores that can be filled with liquid or gas, are in grey. At least a third of the trapped gas is contained with a single large bubble for most of samples. The existence of large trapped bubbles, in combination with the vesicle size distribution, demonstrates that at least the largest gas clusters often extend through multiple pores. Bubbles and vesicles are binned into fifty logarithmically spaced bins and each bin is divided by the total volume of air or vesicles. Volume fraction is not weighted by bin width such that the sum of all bins equals one.

2.3. Comparison to percolation theories

Here we test the hypothesis that percolation theory can describe gas trapping in pumice by fitting Equation (4) to the observed distributions of trapped gas clusters using the maximum likelihood method (Clauset et al., 2009, Iglauer and Wülling, 2016). We find that Equation (4)fits the observed distributions well and that fitted power-law coefficients range from 1.51–2.10, which (other than the coefficient for ML01) are close to the value predicted by percolation theory ($\beta=2.19$) (Fig. 5; Table 1). These power-law fits lend support to a percolation theory treatment of pumice saturation.
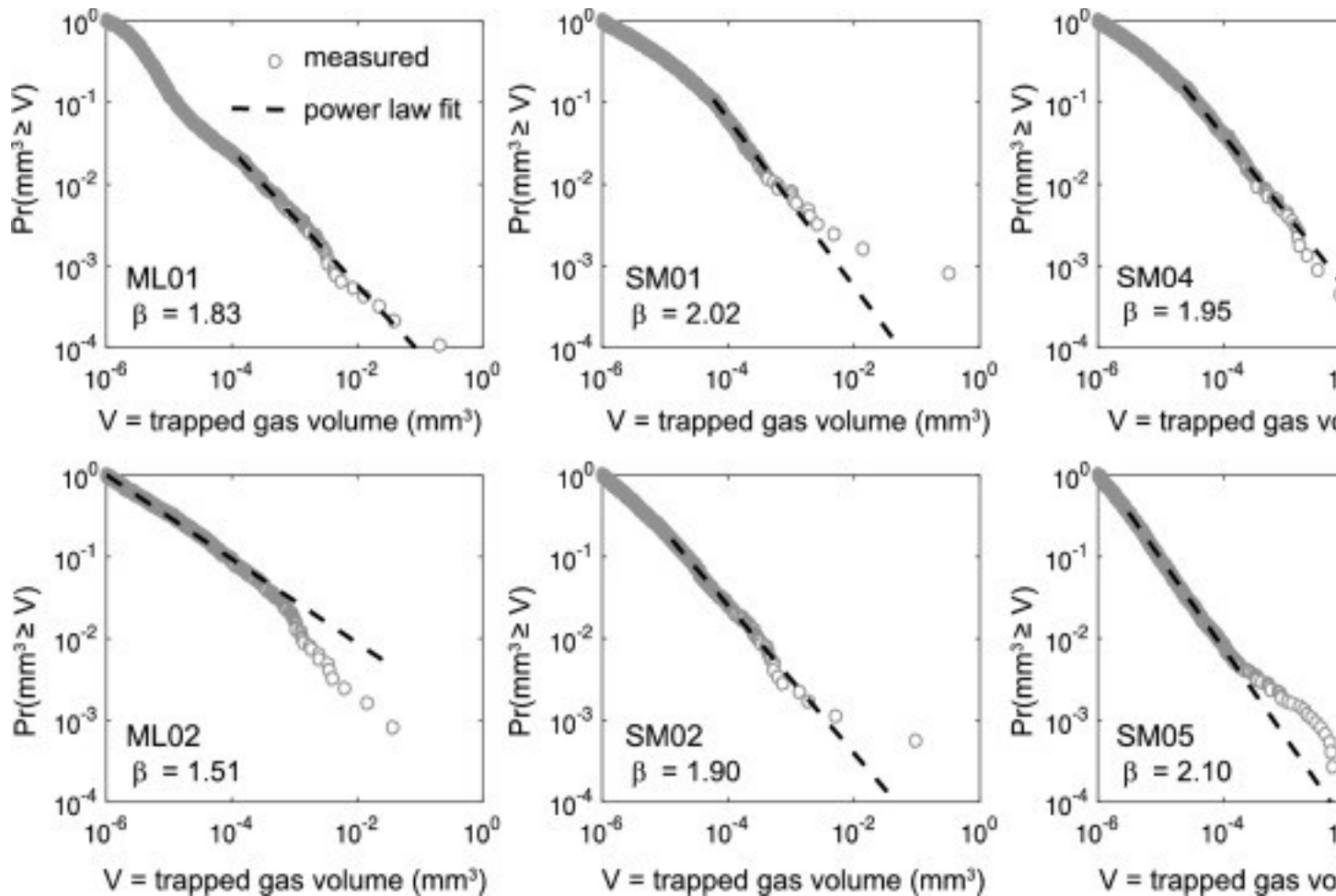
Fig. 5. Power-law fits of bubble-size distributions. Measured distributions of trapped bubble volume (grey circles) and the fitted power-law distributions (dashed lines). The y-axis shows the probability that a bubble is larger than a given volume, V. With the exception of ML02, the fitted power-law coefficients, β, are consistent with the value predicted from percolation theory, $\beta = 2.19$. Because our machine learningsegmentation method generated very small (artifact) bubbles, we removed bubbles smaller than 10^{-6} mm^3 before fitting a power-law coefficient.

Percolation theory also predicts:

$$A \propto V^p,$$

where A is the surface area of the trapped clusters, and V is the volume of the trapped clusters (Stauffer, 1979). From our data sets, we empirically find $p=0.75$–0.83 and the R^2values for these fits are 0.95–0.99 (Table 1 and Fig. S2). Values of p greater than 2/3 demonstrates that the gas bubbles are non-spherical.

3. Mechanisms that cause pumice to sink

The previous sections demonstrated that gas trapping occurs in pumice, that ambient temperature pumice traps more gas than hot (500 °C) pumice, that gas trapping can lead to high enough residual gas saturations to allow pumice to float, and that percolation theory can describe the distribution of trapped gas clusters. The occurrence of gas trapping does not, however, explain why pumice, after floating for days or months, eventually sinks.

3.1. Pumice floatation experiments

To examine why pumice sinks, we conducted pumice floatation experiments using pumice from the 1902 plinian eruption of Santa Maria Volcano, Guatemala. We placed the pumice in artificial seawater and measured the time it took for the pumice to sink. Before the experiments, we cleaned the pumice in an ultrasonicator for four hours and dried the pumice in an oven at 65 °C for 12 h. We specifically chose a temperature lower than 100 °C to ensure that we did not break pumice walls during the drying process and used µXRT to confirm that the pumice was dry prior to experiments. Table 2 shows pumice weights, sizes, and characteristics. While we did not measure the volume of each pumice clast, we estimated volume by assuming porosities of 80% and glass densities of 2.4 g m^{-3}.

Table 2. Floatation time measurements for Santa Maria pumice.

Sample name	Dry weight (g)	Estimated volume (cm³)	Floatation time (days)
SM_F02	0.30	0.63	17.3
SM_F03	0.25	0.53	22.7
SM_F05	0.46	0.95	20.2
SM_F06	0.68	1.42	17.0
SM_F09	0.61	1.28	195.5
SM_F10	0.06	0.13	2.6
SM_F11	0.55	1.15	28.2
SM_F21	0.54	1.12	2.5
SM_F22	0.12	0.24	20.1

To initiate the floatation experiments, we dropped the pumice from a height of 4 cm into individual containers of artificial seawater. These containers were covered to prevent evaporation and contamination. We monitored the pumice with a time lapse camera that could determine when each clast sank to the nearest minute.

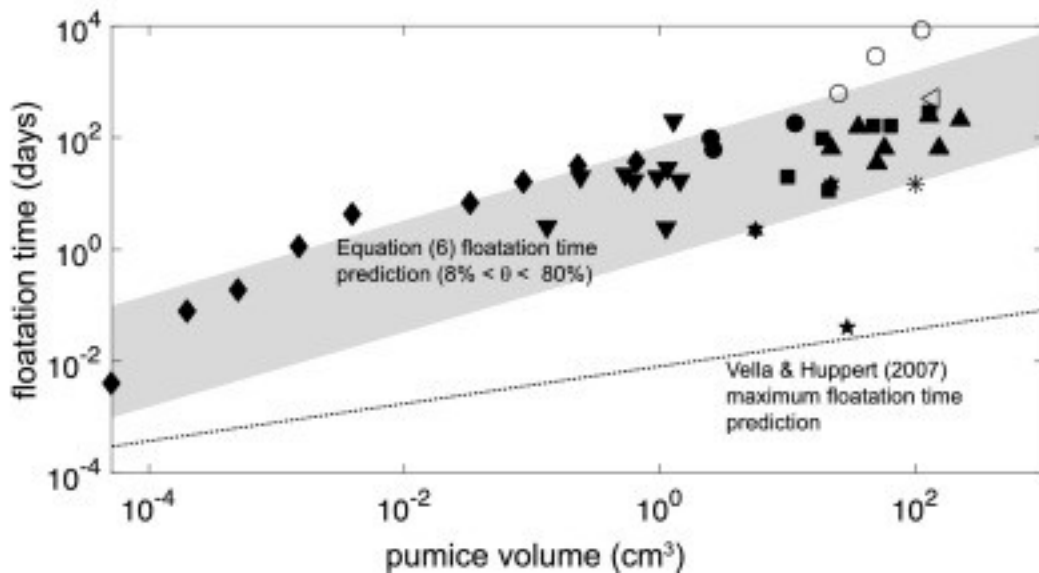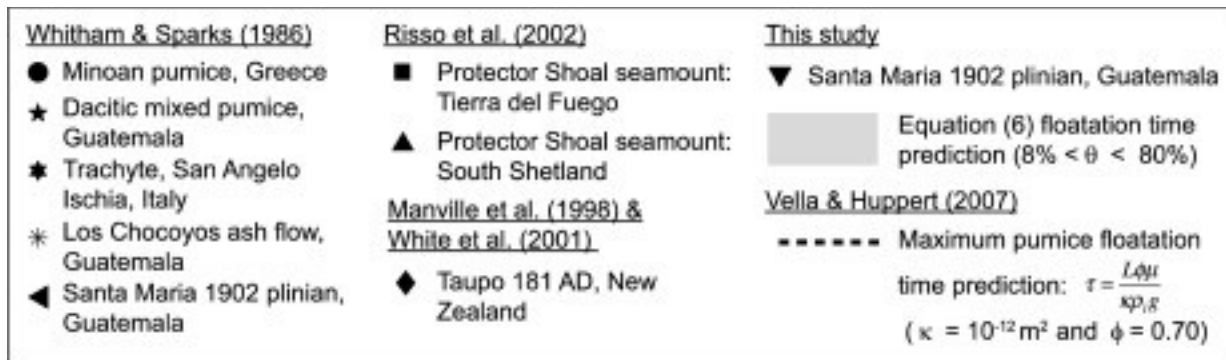## 3.2. Pumice floatation timescale

Here we propose that the diffusion of trapped gas bubbles out of the pumice (and eventually to the atmosphere) causes pumice containing trapped gas clusters to sink. We envisage that the diffusion process is analogous to Ostwald ripening where small (and thus higher pressure) trapped gas clusters diffuse into larger clusters and eventually to the atmosphere. If gas diffusion does control pumice buoyancy through time, then pumice floatation time should scale like a diffusive process where

$$(5) \quad \tau \sim \frac{L^2}{D_{eff}},$$

and where L is the mean diameter of the pumice, and D_{eff} is the effective diffusion coefficient. The effective diffusion coefficient for trapped gas in pumice, as in other porous media, is not just the gas–liquid diffusion coefficient, but should be weighted by the connectivity of the porous media (i.e., porosity and partial saturation). From Hunt et al. (2014) we write effective diffusivity as $D_{eff} = D\theta^2$, where θ is water saturation (fraction of pore space filled by water) and D is the liquid–gas diffusion coefficient, such that

$$(6) \quad \tau \propto \frac{L^2}{D\theta^2}.$$

We test the hypothesis that diffusion of trapped gas out of pumice allows pumice to sink by comparing experimental measurements of pumice floatation time and volume (Whitham and Sparks, 1986, Manville et al., 1998, Risso et al., 2002, White et al., 2001) with Equation (6)and where $L \sim V^{2/3}$ (Fig. 6). Because we do not know θ for any individual pumice, and because, if our hypothesis is correct, θ changes through time, we consider Equation (6) with a range of saturation values (8–80%).

Fig. 6. Floatation time as a function of pumice volume. Measurements of pumice floatation from this study, Whitham and Sparks (1986), Manville et al. (1998), Risso et al. (2002), and White et al. (2001). Pumice floatation time predictions from this study (Equation (6)) and Vella and Huppert (2007) are also shown. Measured floatation times fit the trend predicted by Equation (6) (grey bar). Filled symbols represent measured sinking times while open symbols represent projected sinking times.

1. Download high-res image (363KB)
2. Download full-size image

3.3. Pumice floatation results and model comparison

Fig. 6 shows measurements of floatation time and volume (this study and four others) against predictions from Equation (6) and where D=1.9×10−5cm2s−1 is the air–water diffusion coefficient at room temperature. Experimental measurements of pumice floatation times generally match predictions from Equation (6) (Fig. 6). We also list pumice floatation times from our experiments in Table 2.

It is worth noting, however, that if pumice are highly non-spherical, then we overestimate the effective length scale (shortest pumice axis). Furthermore, the

timescale for pumice floatation may depend strongly on θ, not only because θ affects the diffusivity, but also because more diffusion must occur to sink a pumice with an initially high trapped gas content.

While we are not the first to recognize that pumice floatation time scales like a diffusive process (Manville et al., 1998), diffusion of trapped gas out of the pumice has not previously been identified to be the controlling process. Fig. 6, in combination with observations of gas trapping, suggests that it is the diffusion of trapped gas out of pumice that causes raft and other floating pumice to eventually sink.

4. Discussion

4.1. Gas trapping timescale

We find that water saturation of pumice is a two-step process. First, capillary and hydrostatic pressures drive water into pores. Water invasion often leads to gas trapping (e.g. section 1.1) and ends when there are no longer pores to invade. Second, gas slowly diffuses out of trapped gas pockets thereby creating more space for the liquid (section 3). Here we estimate the timescale for the first of these processes – the time for pumice to reach its residual saturation state.

If pumice can be modeled as a bundle of horizontal parallel cylindrical tubes and capillary pressures drive fluid into the tubes, then the Washburn equation can describe the timescale for water saturation over horizontal distance L,

$$(7) \quad t = \frac{4L^2 \mu}{\gamma d},$$

where d is mean pore throat diameter. Equation (7) suggests that pumice with 0.05 mm diameter pores should reach its residual saturation state very rapidly: 2.7 s for 5 cm pumice and 18 min for 1 m pumice. In other words, if a dry pumice is set on water, then capillary forces draw in liquid quickly and set the wetting pattern and trapped gas geometry in time t. We emphasize that pumice can remain buoyant following water invasion due to gas trapping.

4.2. Water saturation of hot versus cold pumice

We find that residual gas saturation is lower for hot pumice (500 °C) compared to ambient temperature pumice, and that these lower gas saturations can account for the buoyancy differences of hot versus cold pumice (Table 1). Because hot pumice may rapidly saturate due to non-condensable gas contraction (Whitham and Sparks, 1986, Cashman and Fiske, 1991, Allen et al., 2008), we compare the pressure differences generated by three processes that can drive fluid into pumice: water column weight, capillary action, and gas cooling and contraction.

Gravity induces a pressure difference when pumice is submerged in water proportional to

$$(8) \quad \Delta P = (\rho_l - \rho_g)gL \sim 10^3 \, Pa,$$

choosing $L = 10 \, cm$. The pressure difference induced by capillary forces is

$$(9) \quad \Delta P = \frac{2\gamma}{R} \sim 1.5 \times 10^4 \, Pa,$$

where $R = 10 \, \mu m$ is pore throat radius. Lastly, the pressure difference created by gas contraction is proportional to the change in temperature of the gas by the ideal gas law such that

$$(10) \quad \Delta P = P_i \frac{\Delta T}{T_i}.$$

Assuming that the initial pressure, P_i, of the gas is atmospheric ($\sim 10^5 \, Pa$), the initial temperature of the gas, T_i, is 800 K, and the change in gas temperature, ΔT, is 500 K, then $\Delta P \sim 3.7 \times 10^4 \, Pa$.

Gas contraction can thereby produce pressure differences as large as those produced by capillary forces which suggests that, because pressure gradients drive fluid flow, gas contraction can be a relevant process for liquid ingestion. Furthermore, we expect that heat transfer from pumice to liquid is rapid (<1 s) because pumice walls are very thin,

$$(11) \quad t \sim L_w^2 / D_w,$$

where $L_w \sim 10^{-5} - 10^{-6} \, m$ is the glass wall thickness (Fig. 2) and $D_w \sim 10^{-7} \, m^2 s^{-1}$ is water thermal diffusivity. Rapid heat transfer suggests that gas contraction occurs simultaneously with capillary induced pore filling. We note, however, that gas contraction may not proceed prior to pore filling because hot gas must contact cool liquid for heat transfer (e.g., Stroberg et al., 2010).

Following the derivation of the Washburn equation (Equation (7)), we derive a new timescale for the initial stage of water ingestion into pumice when both gas contraction and capillary forces drive fluid flow:

$$(12) \quad t = \frac{4\mu L^2}{R^2 \left(\frac{2\gamma}{R} + P_i \frac{\Delta T}{T_i} \right)}.$$

Gas contraction in hot pumice may help to explain the differences in residual gas saturation of hot and cold pumice. When pressure doesn't change, according to the ideal gas law

$$(13) \quad \frac{V_i}{V_f} = \frac{T_i}{T_f},$$

where V_i and T_i are initial volume and temperature of gas within a pumice and V_f and T_f are final volume and temperature, respectively. We therefore expect that when air is cooled from 800 to 300 K, $V_f = 0.37 V_i$. Our experiments showed that hot pumice contained gas in $\sim 23\%$ of pore space while ambient temperature pumice retained gas in 54–79% of its pore space. This reduction in trapped gas volume

is ~0.23/0.7=0.32 and is approximately the value (0.37) predicted by gas contraction alone.

Trapped bubble size distributions matched [percolation](#) theory for both hot and ambient temperature pumice ([Fig. 5](#)). Invasion percolation theory works by prescribing a capillary entry pressure for each pore and by filling pores from highest to lowest entry pressure. Percolation theory may apply to hot and non-condensable gas-filled pumice because gas contraction introduces a new, yet additive, pressure difference across each pore and thus does not fundamentally change the mechanism for pore filling.

4.3. Bypass versus snap-off trapping

While the fit of Equation [(4)](#) to the measured trapped gas bubble size distributions supports a percolation control on pumice saturation, we have yet to determine if gas is trapped by bypass or snap-off mechanisms. The trapped bubble area-to-volume ratios show that the trapped bubbles are non-spherical ([Table 1](#)). Furthermore, we observe trapped gas within many interconnected pores ([Fig. 3](#)). Because snap-off trapping leads to gas bubbles trapped in single pores (e.g., [Fig. 1](#)), these observations support a bypass trapping mechanism. Furthermore, bypass trapping is topologically favored over snap-off trapping when both are possible.

4.4. Gas diffusion model

In section [3](#) we demonstrated that the slow diffusion of trapped gas bubbles causes pumice to eventually sink. Here we plot solutions to the diffusion equation to examine how pumice floatation time varies as a function of pumice size, porosity, and initial trapped gas saturation. To write a solution to the diffusion equation we make several assumptions: (1) pumice is spherical; (2) the binary water + [gas mixture](#) in pumice can be described as a continuum, (3) initial trapped gas saturation is uniform within the pumice, (4) the [diffusion coefficient](#) is constant, (5) pumice pores are entirely connected, and (6) the pumice is entirely submersed in water. With these assumptions in place, the average saturation ξ (gas volume/pore volume) in a spherical pumice of diameter L, with initial interior gas saturation ξ_i, and with gas saturation equal to zero at the boundaries $\pm L/2$ is

$$(14) \quad \xi(t) = \frac{6\xi_i}{\pi^2} \sum_{n=1}^{\infty} \frac{1}{n^2} e^{-D_{eff} n^2 \pi^2 t / (L/2)^2}$$

([Carslaw and Jaeger, 1959](#), [Manville et al., 1998](#)). Here we let $D_{eff} = D\theta_i^2 = D(1-\xi_i)^2$ (e.g., Equation [(6)](#)). Pumice sinks when its average density is equal to the density of the surrounding liquid such that

$$(15) \quad *(1-\phi)\rho_r + \phi(1-\xi_*)\rho_l = \rho_l,$$

where ρ_r is the density of the solid phase, $*\xi*$ is the gas saturation when a pumice is neutrally buoyant and ρ_l is the liquid density.

By combining Equations (14) and (15) we can calculate pumice floatation time, the time it takes a pumice to reach gas saturation $*\xi*$, as a function of pumice size L, porosity ϕ, and initial gas saturation ξ_i. Fig. 7 shows solutions to Equations (14) and (15) using contours of constant floatation time. Fig. 7 explores how pumice size, porosity, and initial gas saturation affect pumice floatation. We find that high porosity pumice need higher initial gas saturations to float for the same period of time as lower porosity pumice. Pumice size and porosity vary inversely along contours of constant floatation time and, for constant ϕ and ξ_i, larger pumice float longer.
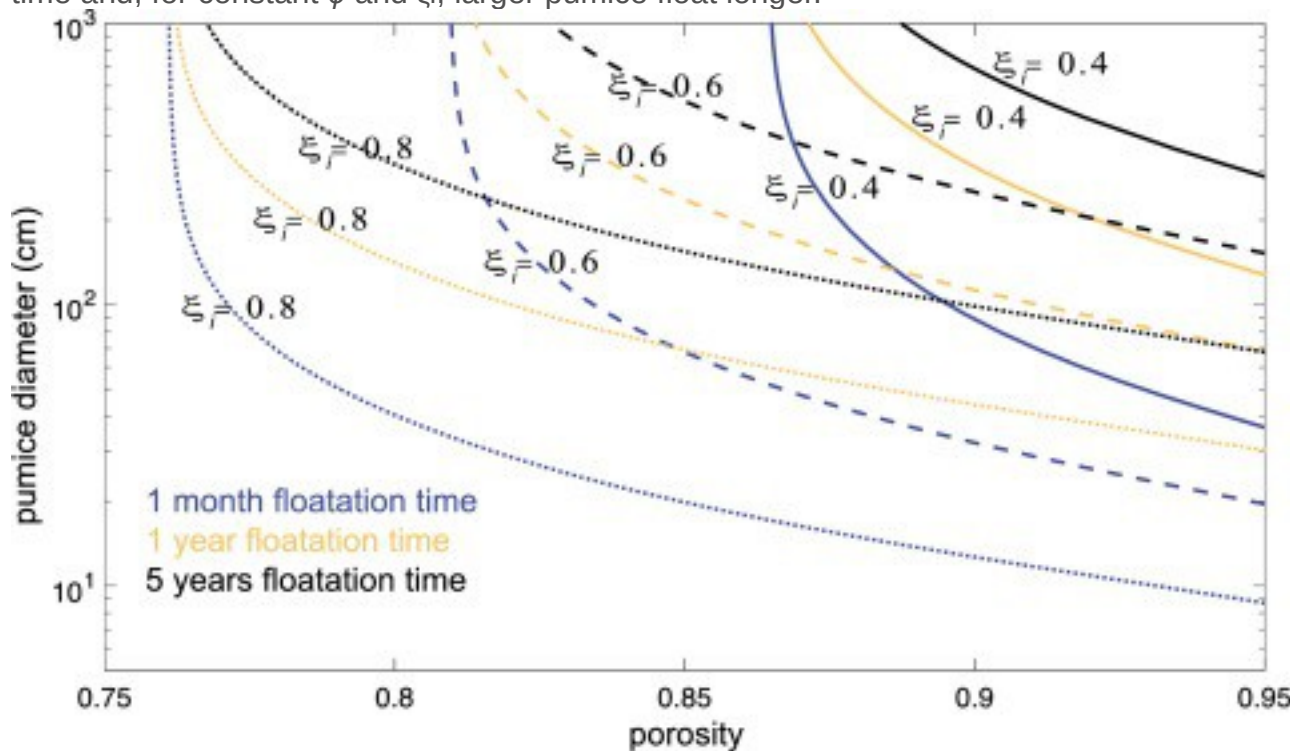
1. Download high-res image (234KB)
2. Download full-size image

Fig. 7. Floatation time as a function of clast size, porosity and initial saturation. We plot solutions to Equations (14) and (15) to demonstrate how floatation time varies with pumice size, porosity, and initial gas saturation, ξ_i. We assume $\rho_r = 2.4$ g cm^{-3}, $\rho_r = 1.0$ g cm^{-3}, and sum the first ten terms of Equation (14).

5. Conclusions

In this paper, we explore the processes that allow pumice to float and sink. To do this, we studied pumice saturation at the scale of pore level processes where capillary forces may be relevant. From estimates of the capillary number – which indicate that surface

tensiondominates over viscous forces in pumice – we hypothesized that pumice can trap isolated gas bubbles as water infiltrates its pores. We used X-ray microtomography to determine if gas trapping occurs in pumice and found that both ambient temperature and hot (500 °C) pumice trap gas. We observed, however, that hot pumice traps far less gas than ambient temperature pumice, consistent with the observation that hot pumice (>300 °C) often sinks after contact with water (Whitham and Sparks, 1986, Allen et al., 2008, Jutzeler et al., 2016). That is, cold pumice can trap enough gas to keep the pumice afloat while gas contraction in hot pumice leads to lower residual gas saturations.

We examined the size distributions of trapped gas in both hot and ambient temperature pumice and found that the distributions fit a power-law prediction from percolation theory. The power-law fits support a percolation theory treatment of water infiltration into pumice.

While trapped gas can buoy pumice, we hypothesized that outward diffusion of the trapped gas clusters causes pumice to eventually sink. We quantified this hypothesis with a model for pumice floatation time in terms of trapped gas diffusion (Equation (6)). To test the gas diffusion hypothesis, we conducted pumice floatation experiments and compared Equation (6) to our results as well as data from four other studies. We found that the observed pumice floatation times match a trapped gas diffusion prediction (Fig. 6). Furthermore, we plot solutions to the diffusion equation on a sphere to explore how pumice porosity, size, and initial gas saturation affect floatation time (Fig. 7).

A mechanistic explanation for pumice floatation is an important step towards understanding when and how pumice is partitioned into rafts versus submarine deposits (e.g., Cashman and Fiske, 1991, Allen and McPhie, 2009; Cas and Giordano, 2014). Indeed, submarine volcanic deposits may not record eruption dynamics because non-condensable (i.e., CO_2 or air) gas trapping can make pumice buoyant. Furthermore, our results suggest that the lifetime of buoyant pumice rafts is not just limited by pumice abrasion (e.g., Carey et al., 2001, White et al., 2001), but also by gas diffusion. Non-condensable gas trapping and diffusion, by controlling pumice buoyancy, are therefore important controls on the transport and fate of pumice in the marine environment and location in the rock record.

Acknowledgments

Appendix A. Supplementary material

The following is the Supplementary material related to this article.

[Download Acrobat PDF file (728KB)Help with pdf files](#)

Supplementary information. S.1 Avizo marker-based watershed vesicle separation methods.

References

[Allen et al., 2008](#)

S.R. Allen, R.S. Fiske, K.V. Cashman**Quenching of steam-charged pumice: implications for submarine pyroclastic volcanism**

Earth Planet. Sci. Lett., 274 (1–2) (2008), pp. 40-49

http://doi.org/10.1016/j.epsl.2008.06.050

[ArticleDownload PDFView Record in Scopus](#)

[Allen and McPhie, 2009](#)

S.R. Allen, J. McPhie**Products of neptunian eruptions**

Geology, 37 (7) (2009), pp. 639-642

[CrossRefView Record in Scopus](#)

[Aveyard and Saleem, 1976](#)

R. Aveyard, S.M. Saleem**Interfacial tensions at alkane-aqueous electrolyte interfaces**

J. Chem. Soc. Faraday Trans. 1, Phys. Chem. Condens. Ph., 72 (1976), pp. 1609-1617

[CrossRefView Record in Scopus](#)

[Benson and Cole, 2008](#)

S.M. Benson, D.R. Cole**CO_2 sequestration in deep sedimentary formations**

Elements, 4 (5) (2008), pp. 325-331

http://doi.org/10.2113/gselements.4.5.325

[CrossRefView Record in Scopus](#)

[Blunt and Scher, 1995](#)

M.J. Blunt, H. Scher**Pore-level modeling of wetting**

Phys. Rev. E, 52 (6) (1995), pp. 6387-6403

http://doi.org/10.1103/PhysRevE.52.6387

[CrossRefView Record in Scopus](#)

[Bryan et al., 2004](#)

S.E. Bryan, A. Cook, J.P. Evans, P.W. Colls, M.G. Wells, M.G. Lawrence, R. Leslie**Pumice rafting and faunal dispersion during 2001–2002 in the Southwest Pacific: record of a dacitic submarine explosive eruption from Tonga**

Earth Planet. Sci. Lett., 227 (1–2) (2004), pp. 135-154

http://doi.org/10.1016/j.epsl.2004.08.009

[ArticleDownload PDFView Record in Scopus](#)

[Bryan et al., 2012](#)

S.E. Bryan, A.G. Cook, J.P. Evans, K. Hebden, L. Hurrey, P. Colls, J. Firn**Rapid, long-distance dispersal by pumice rafting**

PLoS ONE, 7 (7) (2012)

http://doi.org/10.1371/journal.pone.0040583

[Carey et al., 2001](#)

S. Carey, D. Morelli, H. Sigurdsson, S. Bronto**Tsunami deposits from major explosive eruptions: an example from the 1883 eruption of Krakatau**

Geology, 29 (4) (2001), pp. 347-350, [10.1130/0091-7613(2001)](#)

[CrossRefView Record in Scopus](#)

[Carey et al., 2013](#)

R.J. Carey, M. Manga, W. Degruyter, H. Gonnermann, D. Swanson, B. Houghton, M. Patrick**Convection in a volcanic conduit recorded by bubbles**

Geology, 41 (4) (2013), pp. 395-398, [10.1130/G33685.1](#)

[CrossRefView Record in Scopus](#)

[Carey et al., 2014](#)

R. Carey, R. Wysoczanski, R. Wunderman, M. Jutzeler**Discovery of the largest historic silicic submarine eruption**

Eos, Trans. Am. Geophys. Union, 95 (19) (2014), pp. 2012-2014

[Carslaw and Jaeger, 1959](#)

H.S. Carslaw, J.C. Jaeger**Conduction of Heat in Solids**

(2nd ed), Clarendon Press, Oxford (1959)

[Cas and Giordano, 2014](#)

R.A. Cas, G. Giordano**Submarine volcanism: a review of the constraints, processes and products, and relevance to the Cabo de Gata volcanic succession**

Ital. J. Geosci., 133 (3) (2014), pp. 362-377

[CrossRefView Record in Scopus](#)

[Cashman and](#)

Fiske, 1991

K.V. Cashman, R.S. Fiske**Fallout of pyroclastic debris from submarine volcanic eruptions**
Science, 253 (5017) (1991), pp. 275-280
View Record in Scopus

Chatzis et al., 1983

I. Chatzis, N. Morrow, H. Lim**Magnitude and detailed structure of residual oil saturation**
Old SPE J., 23 (2) (1983), pp. 311-326
http://doi.org/10.2118/10681-PA
CrossRefView Record in Scopus

Clauset et al., 2009

A. Clauset, C.R. Shalizi, M.E. Newman**Power-law distributions in empirical data**
SIAM Rev., 51 (4) (2009), pp. 661-703, 10.1137/070710111
CrossRefView Record in Scopus

Degruyter et al., 2010

W. Degruyter, O. Bachmann, A. Burgisser**Controls on magma permeability in the volcanic conduit during the climactic phase of the Kos Plateau Tuff eruption (Aegean Arc)**

Bull. Volcanol., 72 (1) (2010), pp. 63-74

http://doi.org/10.1007/s00445-009-0302-x

CrossRefView Record in Scopus

Dufek et al., 200

J. Dufek, M. Manga, M. Staedter**Littoral blasts: pumice–water heat transfer and the conditions for steam explosions when pyroclastic flows enter the ocean**

J. Geophys. Res., Solid Earth, 112 (B11) (2007)

Geistlinger and M

2015

H. Geistlinger, S. Mohammadian**Capillary trapping mechanism in strongly water wet systems: comparison between experiment and percolation theory**

Adv. Water Resour., 79 (2015), pp. 35-50

http://doi.org/10.1016/j.advwatres.2015.02.010

ArticleDownload PDFView Record in Scopus

Giachetti et al., 2

T. Giachetti, A. Burgisser, L. Arbaret, T.H. Druitt, K. Kelfoun**Quantitative textural analysis of Vulcanian pyroclasts (Montserrat) using multi-scale X-ray computed microtomography: comparison with results from 2D image analysis**

Bull. Volcanol., 73 (9) (2011), pp. 1295-1309

CrossRefView Record in Scopus

Gürsoy et al., 20

D. Gürsoy, F. De Carlo, X. Xiao, C. Jacobsen**TomoPy: a framework for the analysis of synchrotron tomographic data**

J. Synchrotron Radiat., 21 (5) (2014), pp. 1188-1193

http://doi.org/10.1107/S1600577514013939

CrossRefView Record in Scopus

Hall et al., 2009

M. Hall, E. Frank, G. Holmes, B. Pfahringer, P. Reutemann, I.H. Witten**The WEKA data mining software: an update**

ACM SIGKDD Explor. Newsl., 11 (1) (2009), pp. 10-18

http://doi.org/10.1145/1656274.1656278

CrossRefView Record in Scopus

Hunt et al., 2014

A. Hunt, R. Ewing, B. Ghanbarian**Percolation Theory for Flow in Porous Media, Vol. 880**

Springer (2014)

Ide et al., 2007

T.S. Ide, K. Jessen, F.M. Orr**Storage of CO_2 in saline aquifers: effects of gravity, viscous, and capillary forces on amount and timing of trapping**

Int. J. Greenh. Gas Control, 1 (4) (2007), pp. 481-491

http://doi.org/10.1016/S1750-5836(07)00091-6

View Record in Scopus

Iglauer et al., 20

S. Iglauer, A. Paluszny, M.J. Blunt**Simultaneous oil recovery and residual gas storage: a pore-level analysis using in situ X-ray micro-tomography**

Fuel, 103 (2013), pp. 905-914

http://doi.org/10.1016/j.fuel.2012.06.094

ArticleDownload PDFView Record in Scopus

Iglauer and Wülli

S. Iglauer, W. Wülling**The scaling exponent of residual non-wetting phase cluster size distributions in porous media**

Geophys. Res. Lett (2016)

http://doi.org/10.1002/2016GL071298

Jokiel, 1984

P.L. Jokiel**Long distance dispersal of reef corals by rafting**

Coral Reefs, 3 (2) (1984), pp. 113-116

http://doi.org/10.1007/BF00263761

CrossRefView Record in Scopus

Jutzeler et al., 20

M. Jutzeler, R. Marsh, R.J. Carey, J.D.L. White, P.J. Talling, L. Karlstrom**On the fate of pumice rafts formed during the 2012 Havre submarine eruption**

Nat. Commun., 5 (2014), p. 3660

http://doi.org/10.1038/ncomms4660

Jutzeler et al., 20

M. Jutzeler, M. Manga, J.D.L. White, P.J. Talling, A.A. Proussevitch, S.F.L. Watt, M. Cassidy, R.N. Taylor, A. Le Friant, O. Ishizuka**Submarine deposits from pumiceous pyroclastic density currents traveling over water: an outstanding example from offshore Montserrat (IODP 340)**

Geol. Soc. Am. Bull. (2016), Article B31448-1, 10.1130/B31448.1

Klug and Cashm

C. Klug, K.V. Cashman**Permeability development in vesiculating magmas: implications for fragmentation**

Bull. Volcanol., 58 (2–3) (1996), pp. 87-100

http://doi.org/10.1007/s004450050128

CrossRefView Record in Scopus

Klug et al., 2002

C. Klug, K. Cashman, C. Bacon**Structure and physical characteristics of pumice from the climactic eruption of Mount Mazama (Crater Lake), Oregon**

Bull. Volcanol., 64 (7) (2002), pp. 486-501

http://doi.org/10.1007/s00445-002-0230-5

View Record in Scopus

Lenormand and

R. Lenormand, C. Zarcone**Role of roughness and edges during imbibition in square capillaries**

SPE Annual Technical Conference and Exhibition, Society of Petroleum Engineers (1984)

Manville et al., 19

V. Manville, J.D.L. White, B.F. Houghton, C.J.N. Wilson**The saturation behaviour of pumice and some sedimentological implications**

Sediment. Geol., 119 (1–2) (1998), pp. 5-16

http://doi.org/10.1016/S0037-0738(98)00057-8

ArticleDownload PDFView Record in Scopus

Mueller et al., 20

S. Mueller, O. Melnik, O. Spieler, B. Scheu, D.B. Dingwell**Permeability and degassing of dome lavas undergoing rapid decompression: an experimental determination**

Bull. Volcanol., 67 (6) (2005), pp. 526-538

CrossRefView Record in Scopus

Polacci et al., 20

M. Polacci, D.R. Baker, L. Mancini, G. Tromba, F. Zanini**Three-dimensional investigation of volcanic textures by X-ray microtomography and implications for conduit processes**

Geophys. Res. Lett., 33 (13) (2006)

Richards, 1958

A.F. Richards**Transpacific distribution of floating pumice from Isla San Benedicto, Mexico**

Deep Sea Res. (1953), 5 (1) (1958), pp. 29-35, 10.1016/S0146-6291(58)80005-3

ArticleDownload PDFView Record in Scopus

Risso et al., 2002

C. Risso, R.A. Scasso, A. Aparicio**Presence of large pumice blocks on Tierra del Fuego and South Shetland islands shorelines, from 1962 South Sandwich Islands eruption**

Mar. Geol., 186 (3–4) (2002), pp. 413-422

http://doi.org/10.1016/S0025-3227(02)00190-1

ArticleDownload PDFView Record in Scopus

Rust and Cashm

A.C. Rust, K.V. Cashman**Permeability of vesicular silicic magma: inertial and hysteresis effects**

Earth Planet. Sci. Lett., 228 (1–2) (2004), pp. 93-107

http://doi.org/10.1016/j.epsl.2004.09.025

ArticleDownload PDFView Record in Scopus

Rust and Cashm

A.C. Rust, K.V. Cashman**Permeability controls on expansion and size distributions of pyroclasts**

J. Geophys. Res., Solid Earth, 116 (11) (2011), pp. 1-17

http://doi.org/10.1029/2011JB008494

CrossRef

Saar and Manga

M.O. Saar, M. Manga**Permeability-porosity relationships in vesicular basalts**

Geophys. Res. Lett., 26 (1) (1999), pp. 111-114

CrossRefView Record in Scopus

Stauffer, 1979

D. Stauffer**Scaling theory of percolation clusters**

Phys. Rep.-Rev. Sect. Phys. Lett., 54 (1) (1979), pp. 1-74

ArticleDownload PDFView Record in Scopus

Stroberg et al., 2

T.W. Stroberg, M. Manga, J. Dufek**Heat transfer coefficients of natural volcanic clasts**

J. Volcanol. Geotherm. Res., 194 (4) (2010), pp. 214-219

ArticleDownload PDFView Record in Scopus

Tait et al., 1998

S. Tait, R. Thomas, J. Gardner, C. Jaupart**Constraints on cooling rates and permeabilities of pumice in an explosive eruption jet from colour and magnetic mineralogy**

J. Volcanol. Geotherm. Res., 86 (1–4) (1998), pp. 79-91

http://doi.org/10.1016/S0377-0273(98)00075-4

ArticleDownload PDFView Record in Scopus

Vella and Huppe

D. Vella, H.E. Huppert**The waterlogging of floating objects**

J. Fluid Mech., 585 (2007), p. 245

http://doi.org/10.1017/S002211200700715X

CrossRefView Record in Scopus

Voltolini et al., 20

M. Voltolini, D. Zandomeneghi, L. Mancini, M. Polacci**Texture analysis of volcanic rock samples: quantitative study of crystals and vesicles shape preferred orientation from X-ray microtomography data**

J. Volcanol. Geotherm. Res., 202 (1) (2011), pp. 83-95

ArticleDownload PDFView Record in Scopus

von Lichtan et al

I.J. von Lichtan, J.D.L. White, V. Manville, C. Ohneiser**Giant rafted pumice blocks from the most recent eruption of Taupo volcano, New Zealand: insights from palaeomagnetic and textural data**

J. Volcanol. Geotherm. Res., 318 (2016), pp. 73-88

ArticleDownload PDFView Record in Scopus

White et al., 200_

J.D.L. White, V. Manville, C.J.N. Wilson, B.F. Houghton, N.R. Riggs, M. Ort**Settling and deposition of AD 181 Taupo pumice in lacustrine and associated environments**

J.D.L. White, N.R. Riggs (Eds.), Volcaniclastic Sedimentation in Lacustrine Settings, Blackwell Science, Oxford, UK (2001), pp. 141-150, 10.1002/9781444304251.ch7

CrossRefView Record in Scopus

Whitham and Sparks, 1986

A.G. Whitham, R.S.J. Sparks**Pumice**

Bull. Volcanol., 48 (4) (1986), pp. 209-223

CrossRefView Record in Scopus

Wildenschild et al., 2002

D. Wildenschild, C.M.P. Vaz, M.L. Rivers, D. Rikard, B.S.B. Christensen**Using X-ray computed tomography in hydrology: systems, resolutions, and limitations**

J. Hydrol., 267 (3–4) (2002), pp. 285-297

http://doi.org/10.1016/S0022-1694(02)00157-9

ArticleDownload PDFView Record in Scopus

Wilkinson, 1984

D. Wilkinson**Percolation model of immiscible displacement in the presence of buoyancy forces**

Phys. Rev. A, 30 (1) (1984), p. 520

CrossRefView Record in Scopus

Wilkinson, 1986

D. Wilkinson**Percolation effects in immiscible displacement**

Phys. Rev. A, 34 (2) (1986), p. 1380

CrossRefView Record in Scopus

Wilkinson and Willemsen, 1983

D. Wilkinson, J.F. Willemsen**Invasion percolation: a new form of percolation theory**

J. Phys. A, Math. Gen., 16 (14) (1983), pp. 3365-3376

http://doi.org/10.1088/0305-4470/16/14/028

CrossRefView Record in Scopus

Wright et al., 2006

H.M.N. Wright, J.J. Roberts, K.V. Cashman**Permeability of anisotropic tube pumice: model calculations and measurements**

Geophys. Res. Lett., 33 (17) (2006), pp. 2-7

http://doi.org/10.1029/2006GL027224

View Record in Scopus

Wright et al., 2009

H.M.N. Wright, K.V. Cashman, E.H. Gottesfeld, J.J. Roberts**Pore structure of volcanic clasts: measurements of permeability and electrical conductivity**

Earth Planet. Sci. Lett., 280 (1–4) (2009), pp. 93-104

http://doi.org/10.1016/j.epsl.2009.01.023

ArticleDownload PDFView Record in Scopus